Topotactic Metal Organic Chemical Vapor Deposition in Zeolite Y: Structure and Properties of CH_3MY from MOCVD Reactions of $(CH_3)_2MHY$, Where M = Zn, Cd

Mark R. Steele, Peter M. Macdonald, and Geoffrey A. Ozin*

Contribution from the Advanced Zeolite Materials Research Group, Lash Miller Chemical Laboratories, University of Toronto, 80 St. George Street, Toronto, Ontario, Canada M5S 1A1

Received December 15, 1992

Abstract: A mild and controlled synthetic route has been developed that quantitatively incorporates MOCVD-type precursors within the void spaces of zeolite Y. The process is illustrated with respect to the reactions of volatile, molecular dimethylcadmium and dimethylzinc with Brønsted acid sites in zeolite Y. Charge-balance and templating constraints of the host ensure that the sole reaction product CH_3M (M = Cd, Zn) is exclusively housed in the supercages of zeolite Y with spatial and compositional uniformity throughout the entire host lattice. These anchored CH_3M species are perfectly poised for assembly reactions with volatile chalcogenide reagents to form ordered superlattices of II–VI semiconductor nanoclusters. The geometry, site location, and occupancy of anchored CH_3M have been determined by Rietveld analysis of low-temperature synchrotron powder X-ray diffraction data. For samples chemically analyzed as containing 44 CH_3M moieties per unit cell of zeolite Y, almost equal numbers of CH_3M species are found to be anchored via the metal center to framework oxygens at sites II and III, located exclusively in the supercage. The transformation from HY to CH_3MY host has been conveniently monitored by *in situ* mid-IR and far-IR spectroscopy. Distinctive vibrational modes are assignable to intrazeolite $(CH_3)_2M$, anchored CH_3M, and evolved CH_4 species. Room temperature ^{13}C and ^{113}Cd static and MAS-NMR studies of these species reveal that they are undergoing motion on the NMR time scale in the supercages of zeolite Y. Observed NMR chemical shifts are consistent with primary anchoring interactions between the metal center and the oxygen framework for both chemisorbed $(CH_3)_2MNaY$ and anchored CH_3MY species. In the case of the former, ^{23}Na MAS-NMR spectroscopy reveals the existence of a secondary anchoring interaction between supercage site II Na^+ cations and the nucleophilic methyl groups of the $(CH_3)_2M$ guest.

Introduction

In the continuing search for materials exhibiting novel electronic and optical properties, the nanoporosity of zeolite Y, effectively a diamond lattice of 13 Å supercages, has often been exploited as nanoreaction chambers in which to synthesize, organize, and stabilize ordered supralattices of semiconductor nanoclusters[1] (Figure 1). Nanomaterials of this type are predicted to show optical and electronic quantum size effects (QSE's) as a result of the confinement of charge carriers at the level of an exciton wavelength in the corresponding bulk semiconductors.[2] Conditions for the successful observation and practical utilization for QSE's in semiconductors include control over the size, shape, composition, and spatial homogeneity of the constituent nanoscale clusters.[3]

The methods commonly used to incorporate semiconductor nanoclusters within the void spaces of zeolite hosts involve aqueous and melt-ion-exchange[4] as well as the use of volatile precursors.[5] Stucky has shown that the 13 Å supercages of NaY are able to house up to seven $(CH_3)_2Zn$ or $(CH_3)_2Hg$.[6] The advantages of using volatile reagents for this purpose include the large range of available source materials and achievable loading capacity. Here one is not constrained by many of the restrictions inherent in the ion-exchange process, such as limited cation population due to the requirement of cation charge-balance, unwanted hydroxyl groups from water hydrolysis on multivalent cations, and cations buried in inaccessible sites.[7]

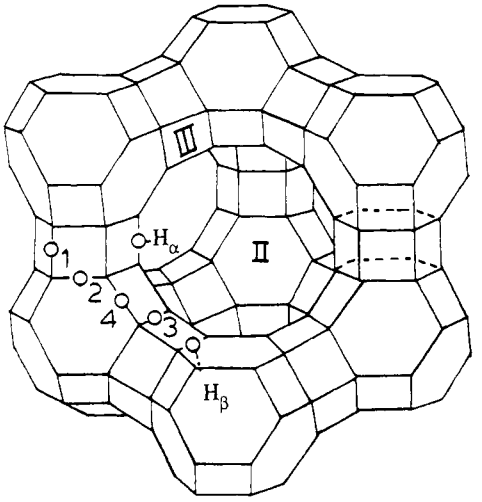

Figure 1. View of zeolite Y centered at the α-cage. Oxygen atoms O(1)–(4), supercage cation sites (II, III), and Brønsted acid sites (Hα, Hβ) are shown.

In this study, topotactic metal organic chemical vapor deposition (MOCVD) is explored as a synthetic pathway to supralattices of semiconductor nanoclusters.[8] Specifically, reactions of volatile $(CH_3)_2M$ MOCVD sources (where M = Zn, Cd) with the Brønsted acid sites in zeolite Y is the focus of this investigation. Preliminary reports of the II–VI semiconductor nanocluster

(1) Ozin, G. A. *Adv. Mater.* **1992**, *4*, 612–649. Ozin, G. A.; Kuperman, A.; Stein, A. *Angew. Chem., Int. Ed. Engl.* **1989**, *28*, 359–376. Herron, N.; Wang, Y.; Eddy, M. M.; Stucky, G. D.; Cox, D. E.; Moller, K.; Bein, T. *J. Am. Chem. Soc.* **1989**, *111*, 530–540 and references cited therein.

(2) Wang, Y.; Herron, N. *J. Phys. Chem.* **1991**, *95*, 525–532. Steigerwald, M. C.; Brus, L. E. *Acc. Chem. Res.* **1990**, *23*, 183–187. Wang, Y. *Acc. Chem. Res.* **1991**, *24*, 133–139 and references cited therein.

(3) Ozin, G. A.; Gill, C., *Chem. Rev.* **1989**, *89*, 1749–1764 and references cited therein.

(4) Stein, A.; Ozin, G. A.; Macdonald, P. M.; Stucky, G. D.; Jelinek, R. *J. Am. Chem. Soc.* **1992**, *114*, 5171–5186 and references cited therein.

(5) Ozin, G. A.; Prokopowicz, R. A. Özkar, S. *J. Am. Chem. Soc.* **1992**, *114*, 8953–8963. Ozin, G. A.; Prokopowicz, R. A.; Özkar, S. *Acc. Chem. Res.* **1992**, *25*, 553 and references cited therein.

(6) Stucky, G. D.; MacDougall, J. E. *Science* **1990**, *247*, 669–678.

(7) Townsend, R. P. *Chem. Ind.* **1984**, 246–251 and references cited therein.

(8) Ozin, G. A.; Özkar, S. *Chem. Mater.* **1992**, *4*, 511–521.

0002-7863/93/1515-7285$04.00/0

materials produced from these kinds of MOCVD reagents have been published in conference proceedings and will be the topic of a subsequent detailed paper.[9,10]

Experimental Section

Mid-IR and far-IR spectra were recorded on self-supporting wafers of zeolite Y mounted within *in situ* reaction cells, having respectively NaCl (4000–400 cm^{-1}) and polyethylene (700–30 cm^{-1}) windows.[11a] Nicolet 20SXB (at a resolution of 2 cm^{-1}) and Nicolet 20F (at a resolution of 4 cm^{-1}) spectrometers were used to collect mid-IR and far-IR spectra of the samples. Low-temperature far-IR spectra were obtained with the wafer mounted on a copper holder, the latter being attached to a Displex closed cycle He refrigeration unit (300–10 K) attached to a high vacuum system. FT-IR spectra were collected by coadding 100 and 500 interferograms for mid-IR and far-IR recordings, respectively.

UV–visible diffuse reflectance spectra were obtained on a Perkin-Elmer 330 spectrophotometer with an integrating sphere attachment that was linked to a computer to digitize the data. Sample spectra were referenced to $BaSO_4$.

^{13}C, ^{23}Na, and ^{113}Cd static and MAS-NMR spectra were recorded on a Chemagnetics CMX-300 instrument using spinning rates of 4–5.5 kHz. ^{13}C chemical shifts were measured relative to $(CH_3)_4Si$, ^{23}Na spectra were referenced to 0.1 M NaCl, and ^{113}Cd spectra were referenced to neat $(CH_3)_2Cd$. Samples were prepared by *in situ* vacuum handling techniques[11b] and transferred *in situ* to zirconia rotors, which were sealed with airtight Kel-F caps.[12] ^{13}C spectra were collected with use of ^1H decoupling during acquisition with a ^{13}C pulse width of 4 μs, a sweep width of 50 kHz, and a pulse delay of 1 s; between 2000 and 5000 scans were collected. ^{23}Na MAS-NMR spectra were obtained with use of a 10 μs pulse width, a sweep width of 50 kHz, and a pulse delay of 0.5 s; 6000 scans were collected. ^{113}Cd spectra were obtained with use of ^1H decoupling during acquisition with a 4 μs ^{113}Cd pulse width, a 1000 kHz sweep width, and a 60 s pulse delay; 76 scans were collected. Lorentzian line broadening applied to the spectra are 25 (^{13}C), 100 (^{23}Na), and 500 Hz (^{113}Cd).

Low-temperature, high-resolution powder diffraction data were collected on a beamline X7A at the Brookhaven National Synchrotron Light Source. Data collection utilized 0.7025 Å radiation for CH_3CdY and 0.7051 Å radiation for CH_3ZnY. The wavelength was calibrated with a Si standard. Intensity was scaled to the ring current of the Synchrotron source by using an ion prechamber to monitor the intensity of the incident beam. A Kevex detector was used to monitor the diffracted X-rays. Step intervals of 0.005° 2θ (CH_3CdY) and 0.01° 2θ (CH_3ZnY) and integration times ranging from 6 to 10 s were used. Samples were rocked at 2° to maximize particle statistics. Further information of the experimental setup is described in detail elsewhere.[13] Samples were sealed in Linderman tubes which were cooled down to 15 K. Rietveld analysis was accomplished using GSAS structural analysis software.[14] Peak shapes were modeled with a psuedo-Voigt function. The location of extraframework cations were determined by refining their positions as located in Fourier maps after initial refinement of the zeolite host structure. wR_p, R_p, and χ^2 were used to monitor the progress of the refinement.[15]

Elemental analyses were performed by Galbraith laboratories. Si, Al, Na, Cd, and Zn were analysed by inductively coupled plasma emission spectroscopy (ICP). Carbon content was analyzed by IR of CO_2 after combustion in an oxygen atmosphere. Elemental analysis shows that the host is charge balanced by $12Na^+$ and $44MCH_3^+$ cations per unit cell.

(9) Steele, M. R.; Ozin, G. A. *J. Am. Chem. Soc.*, submitted for publication.
(10) Steele, M. R.; Holmes, A. J.; Ozin, G. A. *Proc. 9th IZA*, in press. Ozin, G. A.; Bowes, C. L.; Steele, M. R. *Mat. Res. Soc. Ser.* **1992**, *277*, 105–112.
(11) (a) Ozin, G. A.; Baker, M. D.; Godber, J.; Gil, C. J. *J. Phys. Chem.* **1989**, *93*, 2899–2908. (b) Ozin, G. A.; Pastore, H. O.; Poë, A. J. *J. Am. Chem. Soc.* **1993**, *115*, 1215. (c) Ozin, G. A.; Baker, M. D.; Godber, J.; Shihua, W. *J. Am. Chem. Soc.* **1985**, *107*, 1995–2000.
(12) Haw, J. F.; Speed, J. A. *J. Magn. Reson.* **1988**, *78*, 344–347. Haw, J. F.; Richardson, B. R.; Oshiro, I. S.; Lazo, N. D.; Speed, J. A. *J. Am. Chem. Soc.* **1989**, *111*, 2052–2058.
(13) Cox, D. E.; Toby, B. H.; Eddy, M. M. *Aust. J. Phys.* **1988**, *41*, 117–131.
(14) Rietveld refinement, using the Generalized Structure Analysis System, provided by A. C. Larson and R. B. Von Dreele, LANSCE, Los Alamos National Laboratories.
(15) $R_p = \Sigma|I_o - I_c|/\Sigma I_o$, $R_{wp} = (\Sigma w(I_o - I_c)^2/\Sigma[wI_o^2])^{1/2}$, $\chi^2 = \Sigma w(I_o - I_c)^2/(N_{obs} - N_{var})$.

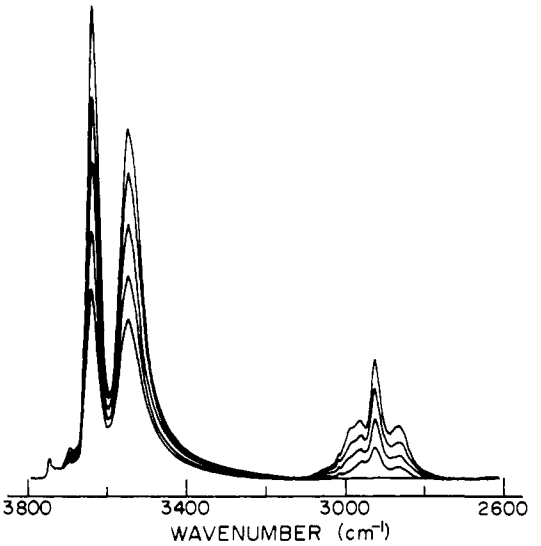

Figure 2. Mid-IR spectra of the titration of charge balancing α- and β-cage protons with $(CH_3)_2Cd$. The decreasing intensity of the ν_{OH} stretching bands (3636, 3546 cm^{-1}) of the zeolite Brønsted acid sites is accompanied by a concomitant increase in that of the ν_{CH} stretching bands (2958, 2900, 2834 cm^{-1}) of the charge balancing CH_3Cd moieties.

Table I. Characteristic Mid- and Far-IR Absorption Bands of CH_3M and $(CH_3)_2M$ in Zeolite HY and NaY

	ν_{CH_3MOZ}, cm^{-1}	ν_{CH}, cm^{-1}
CH_3CdY	61	2958, 2900, 2834
$(CH_3)_2CdNaY$		2960, 2926, 2870
CH_3ZnY	77	2960, 2910, 2836
$(CH_3)_2ZnNaY$		2944, 2894, 2828

Synthesis of CH_3CdY and CH_3ZnY

NH_4Y was prepared by a three-step process: (i) defect removal by slurring NaY in 0.1 M NaCl, followed by thorough washing with distilled, deionized water; (ii) shallow bed calcination in a flow through reaction chamber; (iii) ten successive batch ion-exchanges of NaY slurried in 0.1 M NH_4Cl, washing with copious amounts of distilled deionized water between each exchange. Elemental analysis showed that the zeolite was 80% exchanged with NH_4^+ cations.

Ammonium exchanged zeolite Y was pressed into a thin 30-mg wafer which was placed in an *in situ* cell,[11b] dehydrated, and deamminated with use of a furnace with a preset temperature ramping program: 25–100 °C over 2 h, hold at 100 °C for 2 h, ramp from 100–430 °C over 4 h, and hold at 430 °C for 2 h. The resulting sample is white. The mid-IR spectrum reveals diagnostic ν_{OH_α} (3636 cm^{-1}) and ν_{OH_β} (3546 cm^{-1}) stretching frequencies of α- and β-cage (supercage and sodalite cage) Brønsted acid sites (Figure 2). Dimethylcadmium (vapor pressure 28 Torr, 20 °C) or dimethylzinc (vapor pressure 306 Torr, 20 °C)[16] is added to the zeolite wafer from a bulb reservoir attached to the *in situ* cell. The room temperature reaction may be monitored by *in situ* mid-IR spectroscopy as shown in Figure 2. In this way α- and β-cage protons are quantitatively titrated with $(CH_3)_2M$ to produce the anchored extraframework charge balancing CH_3M species with characteristic ν_{CH} bands as listed in Table I. The reaction stoichiometry may be generally described by the following

$$H_xNa_{56-x}Y + xM(CH_3)_2 \rightarrow (MCH_3)_xNa_{56-x}Y + xCH_4 \quad (1)$$

The methane byproduct is expelled from the hydrophilic zeolite host and is conveniently quantified in the gas phase of the *in situ*

(16) Stringfellow, G. B. *Organometallic Vapour-Phase Epitaxy Theory and Practice*; Academic Press: Boston, 1989; p 25.

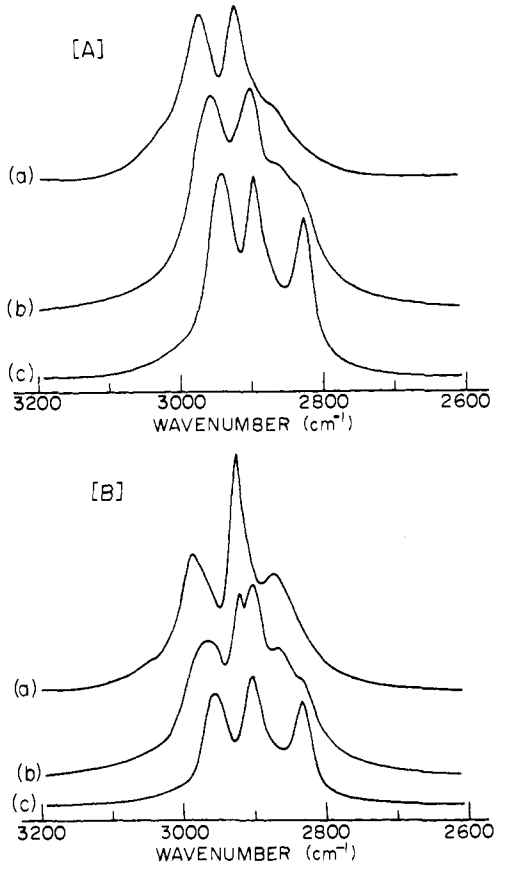

Figure 3. ν_{CH} stretching bands of CH_3MY and $(CH_3)_2MNaY$ species: [A], (a) CH_3ZnY, (b) $(CH_3)_2Zn$ in CH_3ZnY, (c) $(CH_3)_2ZnNaY$; [B], (a) CH_3CdY, (b) $(CH_3)_2Cd$ in CH_3CdY, (c) $(CH_3)_2CdNaY$.

cell. The loss of Brønsted acid sites is found to be directly proportional to the amount of evolved methane. As shown in Figure 2, the Brønsted acid sites may be partially titrated with one $(CH_3)_2M$ reagent. Thus it is possible to complete the titration with another to form, for example, mixed $(CH_3Cd)_x(CH_3Zn)_y$-$Na_{56-x-y}Y$ precursors for subsequent reactions with hydrogen chalcogenides to form mixed (alloy) II–VI semiconductor nanoclusters.

Both mid-IR and far-IR spectroscopy reveal that excess physisorbed $(CH_3)_2M$ is readily removed by room temperature evacuation from CH_3MY, after the Brønsted acid sites in HY have been consumed. This is in contrast to that found for dimethylzinc or dimethylmercury in NaY in which the molecules are strongly chemisorbed.[6] The ν_{CH} stretching modes of the anchored CH_3M groups in CH_3MY are distinctive, arising at higher frequencies than those found for $(CH_3)_2M$ both in NaY or in excess in CH_3MY (Figure 3, Table I).

The far-IR spectra of CH_3M anchored precursors in HY are also distinct from those of their corresponding M^{2+} exchanged forms in zeolite Y as well as chemisorbed $(CH_3)_2M$ in NaY.[17] The diagnostic cation translation modes of M^{2+} sites III, II, I, I′ are absent, and in their place occur lower frequency modes with peak maxima for CH_3ZnY and CH_3CdY at 77 and 61 cm^{-1}, respectively (Figure 4, Table I).

Assuming that the anchored CH_3M species behave vibrationally like charge-balancing point mass local oscillators,[17a] one predicts frequency shifts on passing from site II M^{2+} to CH_3M species to be very close to the ones observed in practice (Figure 4). Moreover, the observed frequency shift observed on passing from CH_3Zn to CH_3Cd anchored species is essentially that predicted using the

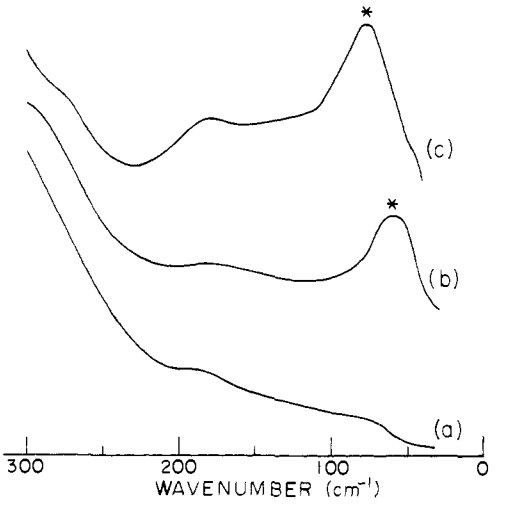

Figure 4. Far-IR spectra of (a) dehydrated HY, (b) CH_3CdY, and (c) CH_3ZnY. Asterisks indicate translatory modes of anchored CH_3M species.

point mass local oscillator approximation. It is noteworthy that the far-IR band assigned to the translatory motion of the CH_3M moieties in the supercages of zeolite Y is quite broad (fwhm ≈ 30 cm^{-1}) and could conceivably conceal the existence of both site II and III anchoring sites (see Rietveld PXRD refinement later). A variable-temperature far-IR study down to 29 K suggested that hot band broadening does not contribute to the observed line width. However, whether the observed line width originates from multiple site occupancy of CH_3MY or other phenomena like residual correlation coupling between or local Si/Al site distributions around CH_3M moieties cannot be determined with the available data.

The far-IR spectrum of $(CH_3)_2CdNaY$ provides some valuable clues concerning the nature of the chemisorbed state of $(CH_3)_2$-Cd in NaY. Dehydrated NaY displays resolved site II, I, I′, and III Na^+ cation translatory modes at 188, 162, 112, and 89 cm^{-1}, respectively.[11c] A neat liquid of $(CH_3)_2Cd$ has a δ_{CCdC} skeletal deformation mode at 140 cm^{-1}.[18] The corresponding data for $(CH_3)_2CdNaY$ show a split, red shifted δ_{CCdC} skeletal deformation mode at 134, 124 cm^{-1} and a slightly red-shifted, broadened and split site II Na^+ cation mode at 186, 174 cm^{-1}, with sites I, I′, and III remaining essentially unchanged. Together these far-IR observations are best interpreted in terms of the anchoring of $(CH_3)_2Cd$ to both oxygen framework and Na^+ cation extra-framework sites with a geometry what removes the degeneracy of these guest and extraframework cation vibrational modes (in line with ^{13}C, ^{113}Cd, and ^{23}Na MAS-NMR and UV–visible spectroscopic data presented below).

Solid-State NMR Spectroscopic Studies of $(CH_3)_2MNaY$ and CH_3MY

^{13}C, ^{23}Na, and ^{113}Cd static and MAS-NMR spectra were obtained for saturation loadings of chemisorbed $(CH_3)_2MNaY$ and fully loaded CH_3MY (Figures 5–7). A listing of the observed chemical shifts and resonance line widths is given in Table II. Chemical shifts are reported with high-field (low-frequency), shielded resonances being designated as negative. The narrow ^{113}Cd line widths observed for the static sample of $(CH_3)_2CdNaY$ relative to various cadmium salts where the chemical shift anisotropies may be 100–190 ppm[19] suggest that the chemical center is undergoing motion on the NMR time

(17) (a) Godber, J.; Baker, M. D.; Ozin, G. A. *J. Phys. Chem.* **1989**, *93*, 1409–1421. Baker, M. D.; Godber, J.; Ozin, G. A. *J. Am. Chem. Soc.* **1985**, *107*, 3033–3043, for Zn^{2+}. (b) M. S. unpublished results for Cd^{2+}.

(18) Butler, I. S.; Newbury, M. L. *Spectrochim. Acta* **1977**, *33A*, 669–680.

(19) Cheung, T. T. P.; Worthington, L. E.; DuBois Murphy, P.; Gerstein, B. C. *J. Magn. Reson.* **1980**, *41*, 158–168.

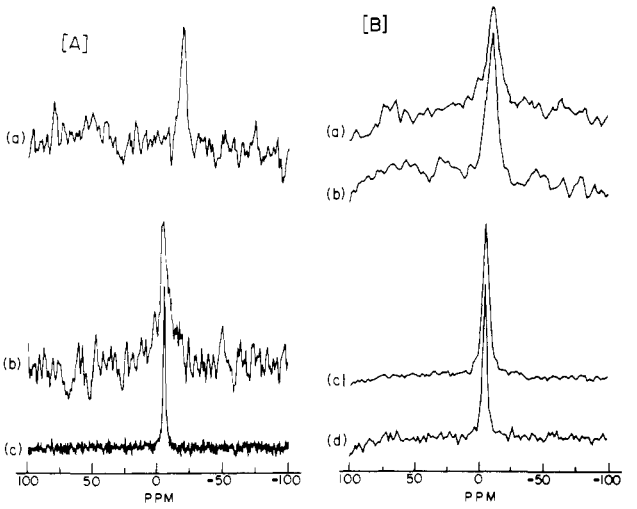

Figure 5. ^{13}C NMR spectra of [A], (A) MAS CH_3ZnY, (b) static $(CH_3)_2$-ZnNaY, (c) MAS $(CH_3)_2ZnNaY$, and [B], (a) static CH_3CdY, (b) MAS CH_3CdY, (c) static $(CH_3)_2CdNaY$, (d) MAS $(CH_3)_2CdNaY$.

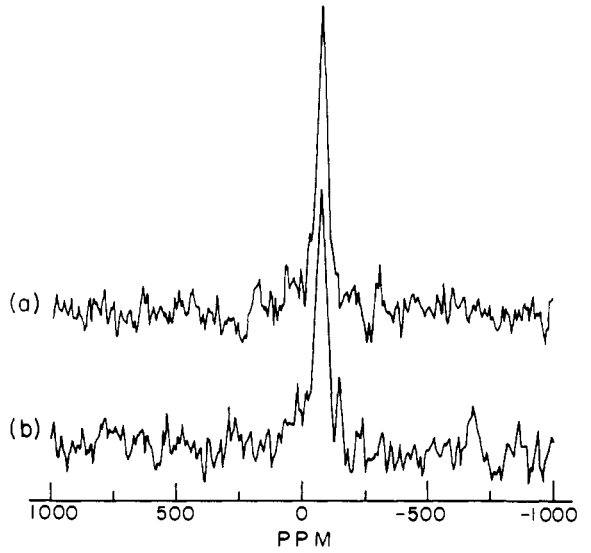

Figure 6. ^{113}Cd NMR spectra of (a) static $(CH_3)_2CdNaY$ and (b) MAS $(CH_3)_2CdNaY$.

Table II. ^{113}Cd and ^{13}C NMR Data for $(CH_3)_2MNaY$ and CH_3MY (M = Zn, Cd)

sample	$\delta^{113}Cd^a$ ($\Delta\nu_{1/2}{}^c$)	$\delta^{13}C^b$ ($\Delta\nu_{1/2}{}^c$)
neat $Cd(CH_3)_2$	0.0 (50)	2.5 (86)
$(CH_3)_2CdNaY$	−75.0 (3000, 3300)	−6.2 (260, 480)
CH_3CdY		−10.8 (660, 770)
neat $Zn(CH_3)_2$		−3.47 (50)
$(CH_3)_2ZnNaY$		−4.9 (120, 530)
CH_3ZnY		−18.2 (420)

[a] Relative to neat $(CH_3)_2Cd$ in ppm. [b] Relative to TMS in ppm. [c] First $\Delta\nu_{1/2}$ in Hz is from MAS spectra, second is from static spectra.

scale.[20] This is further supported by the fact that magic angle spinning did not appreciably narrow the NMR signal. MAS-NMR line widths for crystallographically distinct cadmium species, however, are still narrower, suggesting that the residual line width observed under MAS conditions for $(CH_3)_2Cd$ may be due to a distribution of anchoring supercage sites. A concentration and temperature dependent T_1 and T_2 study of these species, designed to probe details of the intrazeolite dynamical processes in these systems, will be reported in another publication.[21]

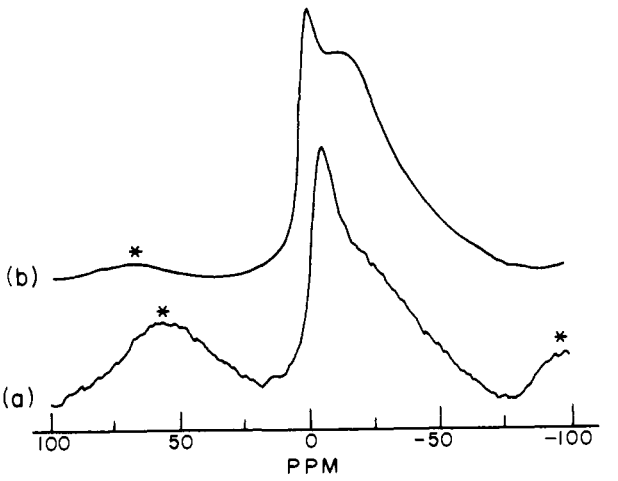

Figure 7. ^{23}Na MAS-NMR spectra of (a) dehydrated NaY and (b) $(CH_3)_2CdNaY$. Spinning sidebands are denoted by asterisks.

The slight shielding, relative to neat $(CH_3)_2M$, of the ^{13}C resonance observed for NaY encapsulated $(CH_3)_2M$ could arise from coordination of the oxygen framework atoms to the metal center, concomitant with a possible bending of the skeleton of the $(CH_3)_2M$ guest away from linearity. This "zeolate" type of anchoring scheme[8] is sketched in Figure 7. Effects of this kind have been postulated to occur for $(CH_3)_2M$ in various oxygen and nitrogen donor solvents.[22] The ^{13}C resonance of the CH_3MY species is shielded further with respect to $(CH_3)_2MNaY$. This likely originates from the attachment of the charge-balancing CH_3M moiety to supercage oxygen framework sites, also in a "zeolate" coordination mode[8] denoted CH_3MOZ (see Rietveld structure later), and the expected delocalization of electron density from these oxygens to the attached methyl group on the metal center.

Additional insight into the structure and bonding of $(CH_3)_2M$ species contained in NaY comes from ^{113}Cd and ^{23}Na MAS-NMR spectroscopy of this system. Specifically, the ^{113}Cd chemical shift observed for $(CH_3)_2CdNaY$ depicts a cadmium nucleus that is more shielded than a 1.0 M solution of $(CH_3)_2Cd$ in THF where the oxygen atom of THF coordinates to the cadmium center.[23] This provides compelling support for the conclusion drawn earlier from IR and ^{13}C NMR spectroscopy, that the cadmium center in $(CH_3)_2Cd$ is anchored to the oxygen framework of the NaY host. Interestingly, the corresponding ^{23}Na MAS-NMR spectrum of $(CH_3)_2CdNaY$ displays a clear enhancement of the intensity of the resonance associated with site II Na^+ cations[24] relative to that observed for the empty NaY host (Figure 8). This implies that anchoring interactions prevail between $(CH_3)_2Cd$ and site II Na^+ cations, as well as the oxygen framework in NaY.

Collectively, the solid-state NMR data portray a picture of $(CH_3)_2CdNaY$ in which the electrophilic cadmium center of $(CH_3)_2Cd$ is coordinated to the oxygen framework of NaY, with simultaneous interaction of the nucleophilic carbon of the methyl group with the site II Na^+ cations, in an anchoring configuration of the type illustrated in Figure 8a. This kind of adsorption, polarization scheme is of the type postulated to occur in the extraframework cation (electric field) induced ionization, charge

(20) Engelhardt, G.; Michel, D. *High Resolution Solid-State NMR of Silicates and Zeolites*; John Wiley & Sons; Toronto, 1987; p 389.
(21) Steele, M. R.; Macdonald, P. M.; Ozin, G. A.,manuscript in preparation.
(22) Soulati, J.; Henold, K. L.; Oliver, J. P. *J. Am. Chem. Soc.* **1971**, *93*, 5694–5698.
(23) Cardin, A. D.; Ellis, P. D.; Odom, J. D.; Howard, J. W., Jr. *J. Am. Chem. Soc.* **1975**, *97*, 1672–1679.
(24) Ozin, G. A.; Özkar, S.; Macdonald, P. M. *J. Phys. Chem.* **1990**, *94*, 6939–6943. Jelinek, R.; Özkar, S.; Ozin, G. A. *J. Am. Chem. Soc.* **1992**, *114*, 4907–4908.

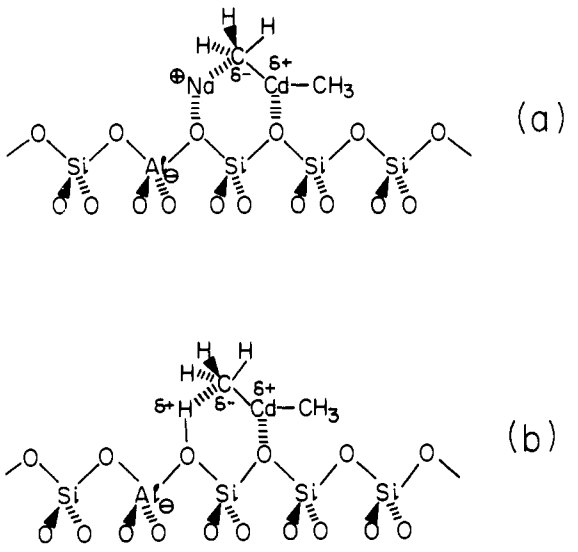

Figure 8. Schematic illustrations of (a) the chemisorption of $(CH_3)_2Cd$ in NaY and (b) the anchoring reaction of $(CH_3)_2Cd$ in HY.

separation processes observed for anhydrous hydrogen halides,[25] hydrogen sulfide,[26] water,[27] propyl halides,[28] and silicon tetrachloride[29] in dehydrated alkali and alkaline earth zeolite Y hosts. An interaction scheme of this type is most probably involved in the protonation of $(CH_3)_2M$ in HY to yield CH_3MY and CH_4, as illustrated in Figure 8b. On a final note, a ^{113}Cd static or MAS NMR signal could not be observed for CH_3CdY, with or without cross-polarization. The T_1 for this material must be at least over 600 s. We intend to explore the supercage dynamics of both of these systems further, especially the kinetics of self-exchange of methyl groups between metal centers[22] which might be envisaged to contribute to the ^{13}C and ^{113}Cd MAS-NMR line widths.

UV-Visible Reflectance Spectroscopic Studies of $(CH_3)_2MNaY$ and CH_3MY

The pervasive use of $(CH_3)_2M$ vapor sources for fabricating II–VI semiconductor multiple quantum well (MQW) and supralattice artificial structures has stimulated many investigations of their surface chemistry, thermal and photochemical properties, and optical spectroscopy.[30] In particular, the most intense allowed low-energy optical excitations of these materials are found in the UV spectral region around 205 and 215 nm for gaseous $(CH_3)_2Zn$ and $(CH_3)_2Cd$, respectively.[31] The molecular orbital structures of these species have also been studied in detail.[31] It is generally agreed that the aforementioned UV absorptions correspond to the transition $X\ ^1\Sigma_g \rightarrow B\ ^1\Pi_u$. This excitation promotes a σ-bonding electron to an essentially nonbonding π-level for the linear configuration of the molecule. The photodissociative nature of this UV excitation is the basis of microlithographic techniques using $(CH_3)_2M$ precursors.[32]

The UV–visible diffuse reflectance spectra of the dehydrated host NaY, $(CH_3)_2MNaY$, and CH_3MY are shown in Figure 9.

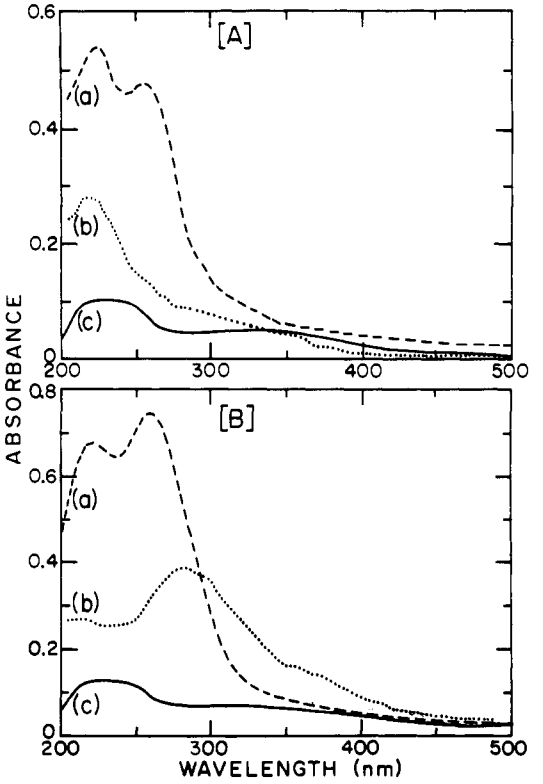

Figure 9. UV–visible reflectance spectra of [A], (a) $(CH_3)_2ZnNaY$, (b) CH_3ZnY, (c) dehydrated NaY, and [B], (a) $(CH_3)_2CdNaY$, (b) CH_3CdY, (c) dehydrated NaY.

Inspection of this set of optical spectra for M = Zn, Cd reveals four noteworthy features:

(i) The optical spectrum of NaY (as well as HY) displays a weak $O^{-II}(2p\pi) \rightarrow Al^{III},Si^{IV}(3d)$ ligand-to-metal charge-transfer band (valence-to-conduction band) around 220 nm.[32]

(ii) The lowest energy absorptions of $(CH_3)_2MNaY$ occur around 250 nm (M = Zn) and 260 nm (M = Cd), both being significantly red-shifted by about 45 nm with respect of their gas-phase analogues. These spectral shifts provide further evidence (see IR and ^{13}C, ^{113}Cd NMR earlier) for the interaction (coordination) of the metal center in $(CH_3)_2M$ with oxygen donor sites of the zeolite framework as illustrated in Figure 8. The effect of bending the linear C–M–C skeleton of $(CH_3)_2M$ can be understood in terms of a Walsh-type molecular orbital scheme.[31] In brief, the degeneracy of the π_u level for $(CH_3)_2M$ is removed and one component a_1^* is stabilized. At the same time, the σ-bonding a_1 level is destabilized. Depending on the relative extent of bending of the CH_3–M–CH_3 skeleton and the strength of the host–guest interactions, the overall effect is a decrease of the energy gap between the original bonding and antibonding levels, causing a red-shift of the lowest energy UV absorption band of $(CH_3)_2MNaY$ compared to that of neat $(CH_3)_2M$, as observed experimentally, Figure 9.

(iii) The lowest energy optical absorption observed for CH_3CdY and CH_3ZnY occurs around 280 and 290 nm, respectively. The band for CH_3ZnY is considerably weaker than that found in CH_3CdY and occurs as a low intensity broad shoulder on the LMCT absorption of the host (Figure 9). This decrease in oscillator strength for the UV absorption of CH_3ZnY compared to that of CH_3CdY parallels that found for $(CH_3)_2Zn$ and $(CH_3)_2Cd$ in the vapor phase. The red-shift of the UV excitations on passing from $(CH_3)_2M$ to CH_3MY probably reflects the change in bonding from CH_3–M–CH_3 to CH_3–M–OZ (see Rietveld structure later). Detailed molecular orbital studies will be required to pin down the electronic origin of this effect.

(iv) Xe lamp UV photoexcitation of CH_3MY ($\lambda_{max} \approx 270$–300 nm) results in the photodissociation of the methyl group, as

(25) Ozin, G. A.; Özkar, S.; Stucky, G. D. *J. Phys. Chem.* **1990**, *94*, 7562–7571.
(26) Karge, H. G.; Raskó, J. *J. Colloid Interface Sci.* **1978**, *64*, 522–532.
(27) Ward, J. W. *Trans. Faraday Soc.* **1971**, *67*, 1489–1499.
(28) Angell, C. L.; Schaffer, P. C. *J. Phys. Chem.* **1965**, *69*, 3463–3470. Angell, C. L.; Howell, M. V. *J. Phys. Chem.* **1970**, *74*, 2737–2742.
(29) Martens, J. A.; Geerts, H.; Grobet, P. J.; Jacobs, P. A. *J. Chem. Soc., Chem. Commun.* **1990**, 1418–1419.
(30) O'Neil, J. A.; Sanchez, E.; Osgood, R. M., Jr. *J. Vac. Sci. Technol. A* **1989**, *7*, 2110–2114. Irvine, S. J. C.; Mullin, J. B.; Giess, J.; Gough, J. S.; Royle, A. *J. Cryst. Growth* **1988**, *93*, 732–743. Yu, C. F.; Youngs, F.; Tsukiyama, K.; Bersohn, R.; Preses, J. *J. Chem. Phys.* **1986**, *85*, 1382–1388.
(31) Chen, C. J.; Osgood, R. M. *J. Chem. Phys.* **1984**, *81*, 327–334.
(32) Rytz-Froidevaux, Y.; Salathé, R. P.; Gilgen, H. H.; Weber, H. P. *Appl. Phys. A* **1982**, *27*, 133–138.
(33) Garbowski, E. D.; Mirodatos, C. *J. Phys. Chem.* **1982**, *86*, 97–102.

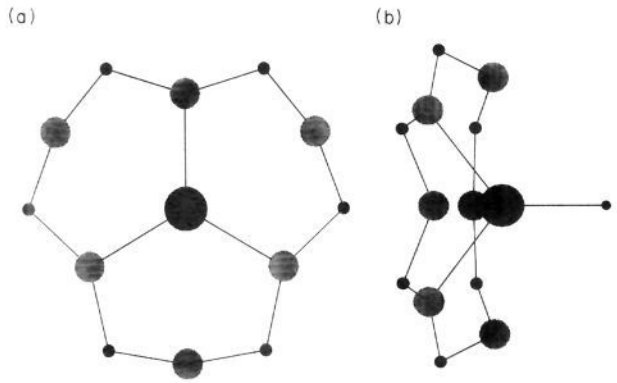

Figure 10. Chem-X view (Rietveld refinement) of anchored CH_3Cd charge-balancing moieties in CH_3CdY at site II in the α-cage: (a) view perpendicular to [1,1,1] and (b) 75° off of [1,1,1]. Large solid spheres represent Cd and Zn, large shaded spheres represent O, intermediate black spheres represent Si/Al, and small black spheres represent C. (Chem-X is a trademark of Chemical Design Ltd.)

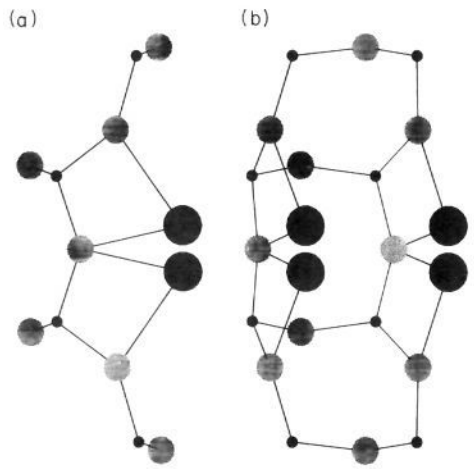

Figure 11. Chem-X view (Rietveld refinement) of anchored CH_3ZnY charge-balancing moieties in CH_3ZnY at site III on the triple-four-ring in the α-cage: (a) perpendicular to [1,0,0] and (b) 60° off of [1,0,0]. Note, all four degenerate site III cations are shown for clarity but the occupancy of this site is only 10%. Large solid spheres represent Cd and Zn, large shaded spheres represent O, intermediate black spheres represent Si/Al, and small black spheres represent C.

determined from *in situ* mid-IR studies of these systems described earlier. In this regard, the photophysical properties of the CH_3–M–OZ anchored species resemble those of the CH_3–M–CH_3 parent molecule,[29,30] implying that the lowest energy excitation of the former is still of the $^1\Sigma_g \rightarrow {}^1\Pi_u$ photodissociative variety.

Rietveld PXRD Structure Refinements of CH_3ZnY and CH_3CdY

A Rietveld refinement of low-temperature synchrotron PXRD data for CH_3CdY and CH_3ZnY reveals two distinct types of anchored guests at supercage locations (Figures 10–12). Observed, calculated, and difference powder patterns are shown in Figure 13. Quite good refinements were obtained for the powder patterns as revealed by low residuals and small χ^2 values[15] (Tables III and IV). These tables also show the symmetry, positions, occupancy, and thermal factors for all atoms in the structures. Table V lists selected bond lengths and angles of the host framework and charge balancing guests. The positions of methyl carbon atoms, located in electron density maps, at site II were constrained in the refinement. Site II located on the six-ring and site III on the triple-four-ring in the supercage are partially occupied. Site II CH_3M moieties are attached to the zeolite framework via three O(2) oxide atoms resulting in pseudotetrahedral symmetry about the metal center (Figure 10). At site III, the CH_3M fragment is anchored by two framework oxygen atoms, O(1) and O(4) (Figure 11). The low occupancy and high degeneracy of site III (192 sites per unit cell) resulted in too low an electron density in the Fourier maps to unequivocally pin down the location of the site III methyl carbon atom (carbon elemental analysis, however, shows that it is present). In fact, the degeneracy and the low local symmetry of site III guests have resulted in very

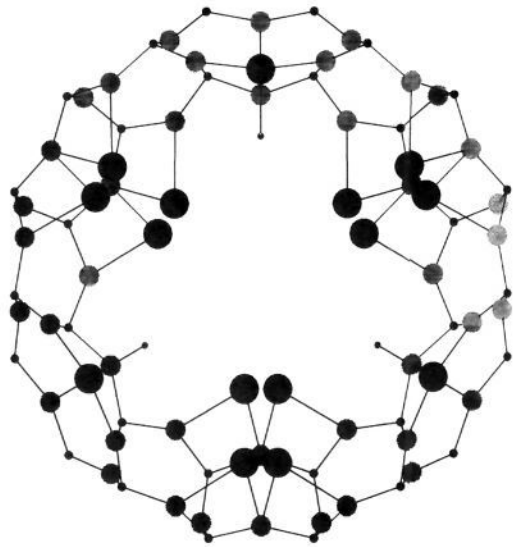

Figure 12. Chem-X view of CH_3ZnY down the 3-fold axis of zeolite Y. The 12-ring aperture is shown, looking into the α-cage. Site III CH_3Zn fragments surround the opening, with site II CH_3Zn fragments at the α-cage six-ring locations. Large solid spheres represent Cd and Zn, large shaded spheres represent O, intermediate black spheres represent Si/Al, and small black spheres represent C.

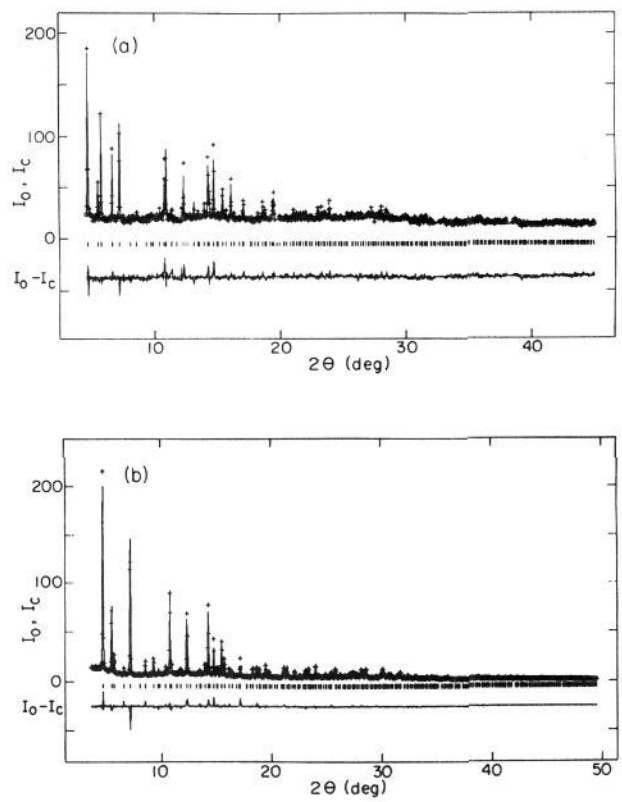

Figure 13. Observed (+, I_o), calculated (—, I_c) and difference ($I_o - I_c$) PXRD patterns (below) of (a) CH_3CdY and (b) CH_3ZnY. Markers show positions of reflections.

Table III. Occupational, Positional, and Thermal Parameters for CH_3ZnY

atom	position	occupancy	*X*	*Y*	*Z*	UISO × 100
Si/Al	192i	1.000(0)	−0.05383(14)	0.12554(16)	0.03620(14)	2.325(86)
O(1)	96h	1.000(0)	0.00000(0)	−0.10693(32)	0.10693(32)	3.40(42)
O(2)	96g	1.000(0)	−0.00360(30)	−0.00360(30)	0.1452(4)	2.81(39)
O(3)	96g	1.000(0)	0.07474(26)	0.07474(26)	−0.0304(4)	2.23(32)
O(4)	96g	1.000(0)	0.07586(33)	0.07586(33)	0.3253(4)	1.43(32)
Zn(II)	32e	0.420(5)	0.23180(15)	0.23180(15)	0.23180(15)	0.32(15)
C(II)	32e	0.420(5)	0.2781(0)	0.2781(0)	0.2781(0)	2.0(0)
Zn(III)	192i	0.103(2)	0.0844(8)	−0.0595(8)	0.4126(7)	10.06(59)

$\chi^2 = 2.576$, $wR_p = 9.80\%$, $R_p = 7.23\%$, $a_o = 24.54410(58)$ Å

Table IV. Occupational, Positional, and Thermal Parameters for CH_3CdY

atom	position	occupancy	*X*	*Y*	*Z*	UISO × 100
Si/Al	192i	1.000(0)	−0.05201(26)	0.12501(23)	0.03677(25)	0.70(2)
O(1)	96h	1.000(0)	0.00000(0)	−0.1081(5)	0.1081(5)	0.40(67)
O(2)	96g	1.000(0)	−0.0016(6)	−0.0016(6)	0.1426(6)	0.15(54)
O(3)	96g	1.000(0)	0.07456(30)	0.07456(30)	−0.0302(5)	−5.1(3.4)
O(4)	96g	1.000(0)	0.0694(6)	0.0694(6)	0.3265(8)	0.38(70)
Cd(II)	32e	0.702(7)	0.24210(12)	0.24210(12)	0.24210(12)	1.0(1.7)
C(II)	32e	0.702(7)	0.2899(5)	0.2899(5)	0.2899(5)	2.0(0)
Cd(III)	192i	0.096(2)	0.0440(8)	−0.0083(10)	0.3924(8)	6.8(6.9)

$\chi^2 = 1.221$, $wR_p = 9.31\%$, $R_p = 7.71\%$, $a_o = 24.53692(44)$ Å

Table V. Selected Bond Distances (Å) and Angles (deg) in CH_3CdY and CH_3ZnY

	CH_3ZnY	CH_3CdY
T(1)–O(1)	1.642(5)	1.696(10)
T(1)–O(2)	1.645(5)	1.614(7)
T(1)–O(3)	1.667(5)	1.637(7)
T(1)–O(4)	1.627(5)	1.692(11)
mean value	1.645	1.660
T(1)–O(1)–T(1)	137.2(8)	132.6(12)
T(1)–O(2)–T(1)	143.5(7)	145.2(13)
T(1)–O(3)–T(1)	136.8(7)	138.5(9)
T(1)–O(4)–T(1)	140.6(8)	129.5(16)
mean value	139.5	136.5
O(1)–T(1)–O(2)	110.8(4)	112.3(8)
O(1)–T(1)–O(3)	111.9(5)	112.6(8)
O(1)–T(1)–O(4)	105.7(5)	99.2(9)
O(2)–T(1)–O(3)	107.3(5)	106.3(7)
O(2)–T(1)–O(4)	112.5(6)	109.3(8)
O(3)–T(1)–O(4)	108.7(6)	117.3(9)
mean value	109.5	109.5
M(II)–O(2)	2.257(9)	2.462(14)
M(II)–C(II)	1.968(6)	2.030(19)
M(III)–O(1)	2.464(25)	2.555(27)
M(III)–O(4)	2.271(18)	2.578(30)

few publications on the crystallographic details of this site. There are three reported positionings of simple M^{q+} cationic guests near the triple-four-ring site, where the cation is able to bond to either one, two, or four framework oxygen atoms. Figure 12 shows CH_3M anchored guests at sites II and III viewed down the 3-fold axis as seen through a 12-ring window looking into the supercage. Residual discrepancies between the observed and difference powder pattern are likely due to unlocated trace amounts of sodium cations and site III CH_3M fragments with different anchoring geometries which are observed in electron density maps but are of too low intensity to refine.

Conclusions

$(CH_3)_2Zn$ and $(CH_3)_2Cd$ are volatile, molecular MOCVD source materials that in NaY anchor through their electrophilic metal centers to oxygen framework (donor) sites and via the nucleophilic carbon center of one methyl group to site II Na^+ (acceptor) cations. By contrast, they react cleanly and quantitatively at room temperature, with Brønsted acid sites in the acid form of dehydrated zeolite Y. The sole products are CH_3ZnY and CH_3CdY, respectively, and stoichiometric equivalents of gaseous CH_4. This kind of topotactic MOCVD process can be controlled by *in situ* mid-IR monitoring of the consumption of Brønsted acid sites, simultaneous growth of CH_3MY, and evolution of CH_4.

Templating constraints and steric restrictions imposed by the zeolite Y host ensure that the reaction product CH_3M is exclusively anchored in the supercage. Charge-balance considerations on replacing Brønsted acid sites by CH_3M entities guarantee spatial and compositional homogeneity of CH_3MY throughout the entire zeolite host lattice. The lower reactivity of the methyl group in CH_3MOZ relative to those in $(CH_3)_2M$ prevents further reaction at RT of CH_3MY to MY. The saturation loading of CH_3M is governed by the populations of Brønsted acid sites in the parent HY. The nucleophilicity (basicity, reactivity) of the methyl groups in the $(CH_3)_2M$ precursors is sufficiently high that both α- and β-cage Brøsted acid sites are made accessible for the anchoring reaction of CH_3M moieties to supercage framework oxygen sites. This results in a maximum possible loading of 56 CH_3M fragments in the unit cell of fully exchanged $H_{56}Y$ (i.e. 7 CH_3M per supercage).

In this particular study, the population of Brønsted acid sites was chosen to deposit close to 6 CH_3M groups per supercage. A low-temperature synchrotron Rietveld PXRD structure refinement of these CH_3MY materials was successful for both M = Zn and Cd and pinpointed essentially equal numbers of CH_3M entities anchored at oxygen framework sites II and III, exclusively located in the supercage of zeolite Y.

This study demonstrates the viability of a mild, clean, and general topotactic synthetic pathway to the self-assembly of uniform arrays of supercage encapsulated MOCVD precursors in a zeolite Y host. Materials of this type are perfectly poised to transform into supralattices of semiconductor nanoclusters. This process has recently been brought to practice for the II–VI semiconductor system to produce periodic arrays of charge-balancing $M_6X_4^{4+}$ nanoclusters, where M = Zn, Cd and X = S, Se,[9,10] housed within the diamond network of 13 Å supercages in the zeolite Y host.

This work serves to bring forth the relationship between MOCVD based semiconductor epitaxy on a planar substrate and semiconductor topotaxy on the internal surface of a zeolite host lattice. We anticipate that topotactic MOCVD methodology of the kind described in this paper will prove to be generally useful

for fabricating two- and three-dimensional quantum confined semiconductor structures in a range of micro- and mesoporous hosts (6 to 1000 Å), for use in ultrasmall and ultradense nanoscale electronic and optical devices.

Acknowledgment. We thank the Natural Sciences and Engineering Research Council of Canada's Operating and Strategic Grants Programmes for financial support of this work. M.R.S. acknowledges NSERC and OGS for graduate scholarship support during the course of this work. The low-temperature PXRD measurements were carried out at the National Synchrotron Light Source, Brookhaven National Laboratories, which is supported by the US Department of Energy, Division of Materials Sciences and the Division of Chemical Sciences. We thank Dr. David Cox for his assistance at Brookhaven National Laboratories and C. Bowes and A. Malek and the rest of our colleagues at the University of Toronto for invaluable discussions during the course of this work.